

On the essential role of SARS-CoV-2 localization in the nasopharynx and intestines in the pathogenesis of COVID-19

Akberdin Ilya R.^{c,d,e}, Afonyushkin Vasiliy N.^{a,b,c}, Kozlova Yulia N.^b, Shchukin Ivan A.^c, Mironova Tatyana E.^{a,g}, Bobikova Anna S.^{a,g}, Cherepushkina Viktoriya S.^a, Donchenko Nikolaj A.^{a,c}, Poletaeva Yulia E.^b, Kolpakov Fedor A.^{d,e,f},

^a Siberian Federal Scientific Center of Agro-BioTechnologies of the Russian Academy of Sciences, 630501, Krasnoobsk, Russia

^b Institute of Chemical Biology and Fundamental Medicine of the Siberian Branch of the Russian Academy of Sciences, 630090, Novosibirsk, Russia

^c Novosibirsk State University, 630090, Novosibirsk, Russia

^d LLC "Biosoft.RU", 630090, Novosibirsk, Russia

^e University Sirius, 354340 Sochi, Russia

^f Federal Research Center for Information and Computing Technologies, 630010, Novosibirsk, Russia

^g Federal State Educational Institution of Higher Professional Education "Novosibirsk State Agrarian University", 630039, Novosibirsk, Russia

Abstract

Patients with COVID-19 may develop pneumonia, severe symptoms of acute respiratory distress syndrome, and multiple organ failure. Nevertheless, the variety of forms of this disease, requires further research on the pathogenesis of this disease. Based on the analysis of published data on the concentrations of SARS-CoV-2 in biological fluids of the nasopharynx, lungs and intestines and using a developed modular model of the virus distribution in human tissue and organs, an assessment of the SARS-CoV-2 reproduction in various compartments of the body is presented. Most of viral particles can enter into the esophagus from nasopharynx. Entering viral particles into the gastrointestinal tract will obviously be accompanied by infection of the intestinal epithelium and accumulation of the virus in the intestinal lumen in an amount proportional their secretory and protein-synthetic activities. The relatively low concentration of SARS-CoV-2 in tissues implies an essential role of transport processes and redistribution of the virus from nasopharynx and intestines to lungs. The model simulations also supposes that sanitation of the nasopharynx mucosa at the initial stage of the infectious process considering inhibition of the virus accumulation by means of cellular and humoral responses has prospects for the use in medicine practice.

Key words: SARS-CoV-2, COVID-19, immunology, nasopharynx, intestines, lungs, mathematical modeling, modular approach, pathophysiology of COVID-19

Introduction

The current state of, and predictions for, the SARS-CoV-2 pandemic constitute unprecedented threats to humanity both in public health and economic terms. The number of people infected with severe acute respiratory syndrome caused by coronavirus 2 (SARS-CoV-2), the causative agent of COVID-19, is growing

rapidly worldwide. Patients with COVID-19 may develop pneumonia [1, 2], severe symptoms of acute respiratory distress syndrome (ARDS), and multiple organ failure [1, 3]. Extraordinary research efforts have taken place to investigate molecular mechanisms of COVID-19 pathogenesis, virus-host interactions and develop effective treatment drugs as well as vaccines in order to curb the spread of the pandemic since early 2020.

Primary contact with the virus occurs mainly through airborne droplets. When inhaled, the main part of the microbial-viral aerosol is deposited on the surface of the nasal mucosa. However, some aerosol particles can enter the trachea and bronchi and multiply in ciliary and secretory cells [4]. Since the upper respiratory tract is quite efficiently capable of eliminating viral particles due to the activity of the mucociliary apparatus, the bulk of the viral particles should enter the nasopharynx. Due to the fact that the virus is firstly able to be released into the external environment by means of the mechanisms of secretion, the role of secreting cells, in particular, cells secreting mucin seems to be decisive in the accumulation of viral particles in the phase of the immune response [4]. The presence of both the ACEII receptor and the serine protease TMPRSS2 in goblet cells also suggests a crucial role in the accumulation of SARS-CoV-2 in the body of mucin-secreting mucous membrane cells [4, 5, 6]. The most intensive synthesis of secreted mucins occurs in the epithelium of the nasopharyngeal region [7], intestines, and salivary glands. It can be assumed that the synthesis and secretion of viral proteins and viral particles should correlate with the activity of the protein-synthetic and secretory apparatus of the cell. The published data on the distribution of SARS-CoV-2 in the body, at the initial stage of the infectious process, seems to be little objective and disputed (controversial). The possibilities of *in vivo* detection of the virus in the human lungs and small intestine are very limited. The analysis of the viral reproduction activity should also take into account the differences in the kinetics of protein synthesis and secretion of cells affected by the virus in different organs and tissues of the organism.

Herein, we describe a new multicompartamental model representing the SARS-CoV-2 *de novo* infection, virus production and distribution among three human organs where the virus is mostly abundant according to the experimental data. The model takes into account action of three different therapies providing more insights into the SARS-CoV-2 pathogenesis and may be *in silico* test site for development of the most effective and precise antiviral therapy. Furthermore, using the sensitivity analysis we have established that the fraction of uninfected target cells is sensitive to different set of parameters depending on the compartment. Results of the analysis suggest a treatment strategy in inactivating the SARS-CoV-2 virus at initial stage of the infection via the nasopharyngeal gate.

Material and methods

Mathematical modeling

The multi-compartmental model of the infectious process has been built using a modular approach implemented in the BioUML platform which supports main standards of the systems biology, modular and visual modeling [8]. In the frame of the approach the biological system is considered as a set of interconnected subsystems or modules. Each module is a mathematical model which can be investigated and simulated independently. Integration of these modules results in a more complex model of the whole system. Modules may leverage different mathematical formalisms and scales and may be viewed as replaceable parts. Modules provide explicit interfaces (variables and constant parameters) represented by ports and through which they can be connected without exposing their inner structure. According to the methodology of the model development process, the presented integrated model and all submodels have been constructed as visual diagrams, where each component of the diagram represents a corresponding mathematical object like

variable, reaction, equation. The visual representation as well as defined properties of diagram elements are the basis for automatic generation of the corresponding Java code that is used to simulate the model in BioUML. All methodological details on visual modular modeling implemented in the platform are presented in the recent publication [9].

The modular model describes the accumulation and degradation of viral particles in the nasopharynx, intestines and lungs, including the transport processes of viral particles along the gastrointestinal tract and circulatory system, which also affect dynamics of changes in the viral load in these organs (or compartments in the model) of the body.

The developed model consists of five modules: three modules represent the infection of sensitive cells with the SARS-CoV-2 virus and its reproduction in the corresponding compartment (nasopharynx, NP; intestine, Intestine; lungs, Lung), and two virus transport modules from NP to Intestine and Lung (Transport from NP to Intestine and Lung) and through the bloodstream from Intestine to Lung (Transport from Intestine to Lung) (Fig. 1).

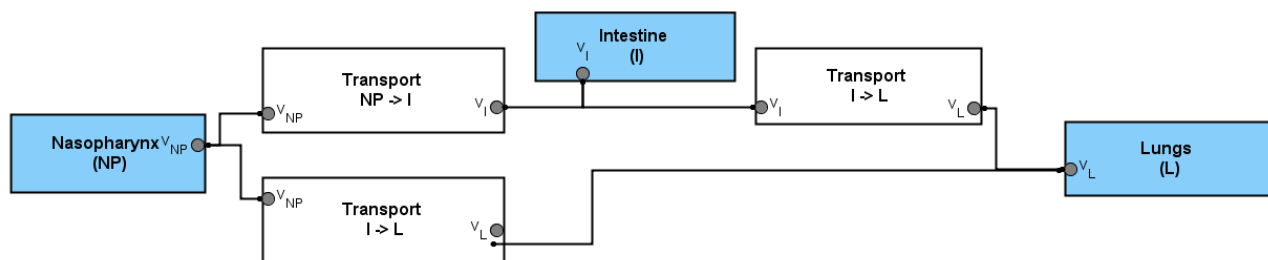


Fig. 1. The developed multicompartmental model of the SARS-CoV-2 infection processes and distribution among three human organs taking into account the virus reproduction in each compartment and viral transport between them. Gray circles are contact ports representing the interface of the module through which it can be connected with other modules or with the integrated model itself.

In each compartment, the model describes the primary entry of the virus into the compartment, the change in the proportion of susceptible cells (which decreases over time, as the cells become infected with the virus) and the number of viral particles due to the processes of replication, degradation and transport of the virus from/to other compartments (Fig. 2). The kinetic laws of the simulated processes and majority of the parameter values originated from the recently published quantitative model used to compare within-host SARS-CoV-2, MERS-CoV, and SARS-CoV dynamics [10].

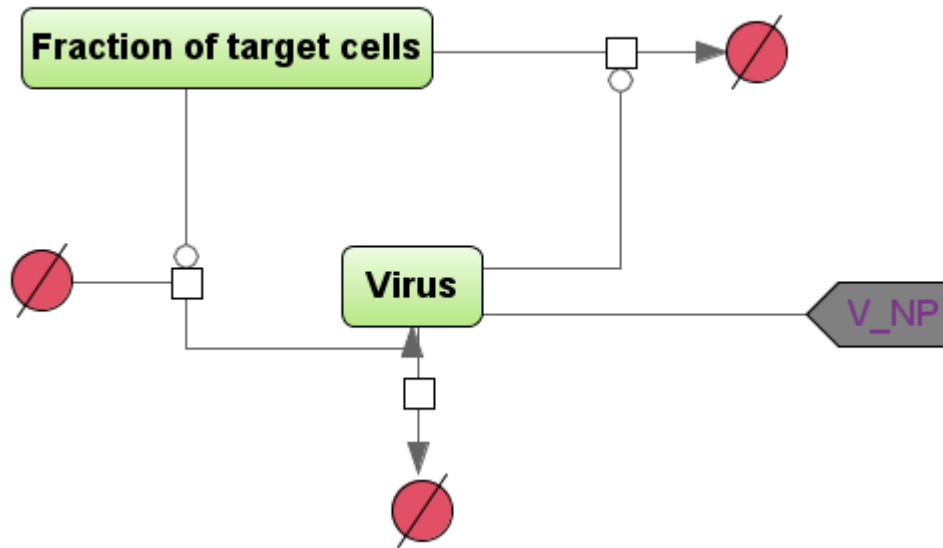


Fig. 2. Schematic diagram describing the multiplication and inactivation of the virus in a certain compartment (the NP module is shown as an example), in the SBGN format [8]. "Fraction of target cells" is the proportion of cells sensitive to the infection, "Virus" is the number of viral particles in a given compartment of the model. The vertices in the bipartite graph in the form of white squares correspond to the reactions in the model, the rate equations of which are given below in the system of ordinary differential equations. To account for the transport of viral particles from the NP module to the Intestine and Lung, a "contact"-type port (gray colour) is used within the modular approach in BioUML.

The developed modular model of the virus infection and distribution between three compartments is described as a system consisting of six differential equations with delay arguments and 22 kinetic parameters (Table 1):

$$\frac{df_{np}}{dt} = -(1 - \epsilon * H_1) * \beta_{np} * f_{np} * V_{np}$$

$$\frac{dV_{np}}{dt} = (1 - \epsilon * H_1) * (1 - \eta * H_2) * \gamma_{np} * f_{np} * V_{np}(t - \tau_{r_{np}}) - \frac{1}{1 - \theta * H_3} * \delta_{np} * V_{np}(t - \tau_{d_{np}}) - K_{tr_{npI}} * V_{np}(t - \tau_{t_{npI}}) - K_{tr_{npL}} * V_{np}(t - \tau_{t_{npL}})$$

$$\frac{df_I}{dt} = -\beta_I * f_I * V_I$$

$$\frac{dV_I}{dt} = K_{tr_{npI}} * V_{np}(t - \tau_{t_{npI}}) + (1 - \epsilon * H_1) * (1 - \eta * H_2) * \gamma_I * f_I * V_I(t - \tau_{r_I}) - \frac{1}{1 - \theta * H_3} * \delta_I * V_I(t - \tau_{d_I}) - K_{tr_{IL}} * V_I(t - \tau_{t_{IL}})$$

$$\frac{df_L}{dt} = -\beta_L * f_L * V_L$$

$$\frac{dV_L}{dt} = K_{tr_{npL}} * V_{np}(t - \tau_{t_{npL}}) + K_{tr_{I_L}} * V_I(t - \tau_{t_{I_L}}) + (1 - \epsilon * H_1) * (1 - \eta * H_2) * \gamma_L * f_L * V_L(t - \tau_{r_L}) - \frac{1}{1 - \theta * H_3} * \delta_L * V_L(t - \tau_{d_L})$$

Where:

np, L, I - nasopharynx, lungs, and intestines, respectively;

β_i - the rate constant of the virus infection in the corresponding compartment;

γ_i - the maximum rate constant of the virus replication depending on the compartment;

δ_i - the death rate of infected cells (and viral particles in these cells, respectively);

f_i - the proportion of cells sensitive to infection;

V_i - the number of viral particles in the corresponding compartment;

$\tau_{ri}, \tau_{di}, \tau_{ti}$ - time delay parameters associated with the processes of replication and assembly of the viral particles; degradation of infected cells and viral particles, including the impact of cellular and humoral immune-mediated responses; transport of viral particles from one compartment to another ($\tau_{r_{npI}}$ - transport from NP to Intestine; $\tau_{r_{npL}}$ - transport from NP to Lung; $\tau_{r_{IL}}$ - transport from Intestine to Lung), respectively;

ϵ, η, θ - constants of the effectiveness of external and/or additional factors limiting the infectious process ($0 < \epsilon, \eta, \theta < 1$): $\epsilon = 1$ corresponds to the complete suppression of the mechanisms of cell infection; $\eta = 1$ reflects 100% efficiency of the inhibition of viral replication and assembly of viral particles in infected cells; $\theta = 1$ denotes the cytotoxic activity of effector T cells/drugs.

H_1, H_2, H_3 - Heaviside step functions, i.e. $H(t) = 0$ if $t < t'$; otherwise $H(t) = 1$; where t' corresponds to the inhibition of infection, replication and assembly of viral particles, activation of the cytotoxicity of an infected cell, or a combination of these factors.

Table 1. Kinetic parameters of the modular model of SARS-CoV-2 infection and distribution between the three compartments.

Parameter	The value	Units of measure	References
β_{nf}	$5.2 * 10^{-6}$	(copies/ml) ⁻¹ *days ⁻¹	[10]
β_I	$5.2 * 10^{-6}$	(copies/ml) ⁻¹ *days ⁻¹	assumption [10, 11, 12]
β_L	$5.2 * 10^{-6}$	(copies/ml) ⁻¹ *days ⁻¹	assumption [10, 11, 12]
γ_{nf}	4.0	day ⁻¹	[10]

γ_I	5.0	day ⁻¹	assumption
γ_L	1.0-2.0	day ⁻¹	assumption
δ_{nf}	0.23 - 0.93)	day ⁻¹	[10]
δ_I	0.46	day ⁻¹	assumption [11]
δ_L	0.046	day ⁻¹	assumption [12]
V_{nf}	100-100000	copies/ml	assumption
$\tau_{r_{nf}}$	0.05	day	[13]
τ_{r_I}	0.05	day	[13]
τ_{r_L}	0.05; 0.5 h (replication) +1 h (budding) = 0.0625 days	day	[13]
$\tau_{d_{nf}}$	0.1	day	assumption
τ_{d_I}	0.1	day	assumption
τ_{d_L}	0.1	day	assumption
$\tau_{t_{npI}}$	0.05	day	assumption
$\tau_{t_{npL}}$	0.05	day	assumption
$\tau_{t_{lL}}$	0.05	day	assumption
$K_{tr_{npI}}$	0.6	day ⁻¹	assumption, [14]
$K_{tr_{npL}}$	0.03-0,00048	day ⁻¹	assumption/experimental model

K_{trI_L}	0.03- 0,0001	day ⁻¹	assumption; experiment
θ_I	0.3-0.8	dimensionless	assumption
θ_L	0.8	dimensionless	assumption
θ_{NP}	0.53-0.8	dimensionless	assumption
ϵ_I	0.5-0.995	dimensionless	assumption
ϵ_L	0.9-0.995	dimensionless	assumption
ϵ_{NP}	0.7-0.995	dimensionless	assumption
$time_{\theta_I}$	13	day	[15]
$time_{\theta_L}$	8	day	
$time_{\theta_{NP}}$	6	day	[15]
$time_{\epsilon_I}$	1-14	day	
$time_{\epsilon_L}$	9	day	
$time_{\epsilon_{NP}}$	1-7	day	[15]

Besides the use of previously published kinetic parameters' values (Table 1), we employed expert evaluation for unknown parameters in order to fit the simulated viral load dynamics to experimental data [10]. The value of the maximum rate constant for viral replication in the nasopharynx, γ_{np} was originated from the study [10] and equals 4.0 day⁻¹, while the parameter value in the intestine was higher (5.0 day⁻¹) due to greater ability of the intestinal mucosa to protein synthesis and cell division [11]. The maximum constant rate for viral replication in the lung has to be 10 times less than in the intestine. However, the parameter value in the lung was increased (Table 1) due to the model does not consider a significantly lower rate of the viral elimination from the lung alveoli.

ϵ indicates reactions of the humoral immune response and the time of its activation's initiation, $time_{\epsilon}$ differs between compartments depending on the time frame of the virus emergence in corresponding compartments. The virus appears in the lung later than in the nasopharynx that supposes delayed humoral response in this compartment. The time frame of the response initiation in the intestine specifies as the most late due to the substantial probability of the immune response by type of nutritional tolerance because of T-regulatory lymphocytes accumulation.

θ represents T-cellular immune response. The order of the response corresponds to the humoral responses order in investigated compartments. The time frames of the T-cellular response in each module are earlier than for the humoral response because the process of antibodies accumulation requires more time.

Values of ϵ and θ parameters depend on the compartmental identity in the manner: $i_{Lung} > i_{NP} > i_I$, where $i \in (\epsilon; \theta)$, while values of the δ parameters depend on the identity in the opposite manner: $i_I > i_{NP} > i_{Lung}$. The greatest value of the parameter is in the intestine due to the initially fast renewal rate of the intestinal mucosa (no more than three days), while the parameter value in the nasopharynx is lower because of lesser renewal rate of multilayered epithelium.

Transport rate constant K_{tr} for the virus transport from the nasopharynx to intestine limited only by virus preservation in the acidic gastric medium [16] has the greatest value, while the parameter value of the virus transfer from the intestine to the lung via blood and lymphatic systems was experimentally measured (see below). The value of K_{tr} representing transport from the nasopharynx to the lung is lesser than in the intestine due to more pronounced barrier properties of the nasopharynx mucosa compared to the intestinal.

Model simulation and sensitivity analysis in BioUML

We numerically solved the model equations by using an ordinary differential equation JNode solver built-in the BioUML with default settings and time increment equals to 0.1 day. Sensitivity analysis [17] implemented in the platform was utilized to investigate the effect of parameter change on the model solution considering the target cell ratio (f_i) in each model compartment as target variables (Table 1). According to the basic, the method calculates sensitivity measures associated with the steady state of a spatially homogeneous reaction system:

$$\frac{dc}{dt} = f(c, k, t) \quad c(0) = c^0$$

where c is the n -vector of concentrations and k is the m -vector of system parameters, while t (time) is the variable of integration. In this case, the local unscaled sensitivities $\frac{\partial c}{\partial k_i}$ are calculated via finite difference approximations:

$$\frac{\partial c}{\partial k_i} = \frac{c_{ss}(k_i + \Delta k_i) - c_{ss}(k_i)}{\Delta k_i}$$

where $c_{ss}(k_i)$ and $c_{ss}(k_i + \Delta k_i)$ indicate solutions of the algebraic systems $f(c, k_i)$ and $f(c, k_i + \Delta k_i)$ correspondingly, while the scaled sensitivities are calculated by multiplying each component $\frac{\partial c}{\partial k_i}$ of the vector $\frac{\partial c}{\partial k_i}$ by the normalization factor $\frac{k_i}{c_{ss}(k_i)}$. As a result of the analysis, we used the scaled sensitivity measures (see below).

Mathematical modeling of sanitation with virucidal medications of the nasopharynx and intestines

To investigate the effect of sanitation by virucidal medications in different compartments of the body on the viral dynamics, we increased the value of parameter ϵ up to 0.995 indicating 99.5 % efficiency of the *de novo* infection blocking and set the time frame of its activation to the first day post-infection (in nasopharynx only (Case 1) and in both compartments (Case 2). To computationally estimate the effect on the outcome of the dynamics, simulations were performed using different initial infection doses: from 10^2 to 10^6 viral particles.

Evaluation of the transfer efficiency of model viral particles from the nasopharynx to the esophagus and trachea, with airborne infection

Spraying of the bacteriophage MS2 virus, which is used as a model virus for airborne transmission of SARS-CoV-2 [15], was performed on Balb/c mice (n=12) in an aerosol chamber with a volume of 1 m^3 . An nebulizer NEB Pro (MicroLife) was used to generate the aerosol. The average droplet size was $10.15 \text{ }\mu\text{m}$. 9 ml of bacteriophage MS2 suspension at a concentration of 2×10^8 PFU/ml had been sprayed for 40 minutes. The final concentration of the bacteriophage was 1.8×10^6 PFU/litre of the air.

The culture of *E. coli* CEMTK 3877 (collection of extremophilic microorganisms of ICBFM) was used as a test strain.

One group of mice (Balb/c, males, n=6) were taken out of the experiment post 1 hour after bacteriophage spraying, while the second one (n=6) was taken out of the experiment post 2 hours and 30 minutes after the spraying. The trachea, esophagus and lung were taken, blood samples were also taken from the left and right ventricles of the heart, the average time for sampling was 15 minutes. The organ was homogenized using ceramic beads, serial dilutions of the homogenate were made. The bacteriophage concentration was determined by the Gracia method.

Experimental evaluation of the efficiency of viral particles transport from the intestines to the lungs through the circulatory and lymphatic systems

Bacteriophage ph 57 (deposited in the collection of Extremophilic Microorganisms and Type Cultures of the Institute of Chemical Biology and Fundamental Medicine of the Siberian Branch of the Russian Academy of Sciences, registration number WFCC #974) [19] was used as an *in vivo* model to assess the efficiency of transport of viral particles from the intestines [18] to the lungs circulatory system - $\square\square\square\square$, while *P. aeruginosa* (WFCC #670) cell culture was employed to determine phage particle activity. The bacteriophage was once administered intragastrically to Balb/c mice (n=12) using a special probe at a dose of $200 \text{ }\mu\text{l}$ per animal. The initial concentration of the bacteriophage was 1.8×10^8 PFU/ml. A group of mice was taken out of the experiment after 2 hours. The organs were homogenized using ceramic beads, serial dilutions of the homogenate were made. The residual concentration of bacteriophage inoculations was determined in 10-fold dilutions. The survival rate of phage particles was determined by the method of two-layer agar (Grazia method). The studies were carried out at room temperature ($30 \pm 2 \text{ }^\circ\text{C}$). All experiments were performed in triplicate.

Statistical data processing

The data were processed by the methods of variational and nonparametric statistics. The level of statistical significance of differences was assessed using Student's t-test and Mann Whitney (p-value < 0.05 was considered as statistically significant).

Approval of animal experiments by the ethical committee

The experimental protocol involving animals was reviewed and approved by the Ethical Committee of Novosibirsk State Agrarian University of Siberian Federal Scientific Center of Agro-BioTechnologies of the Russian Academy of Sciences CM K PO 15-01-2019/No.3 of 10.03.2021.

Results

Viral particles distribution in trachea, lungs and esophagus after airborne infection

After contact of mice with an aerosol of a model virus (bacteriophage MS2) at the initial concentration of 1.8×10^6 PFU/L, the bacteriophage concentration statistically significantly decreases by 0.61 Log₁₀ ($U_{emp} = 3$ (p-value < 0.01)) post 1.5 hours as follows from Table 2. The data allow us to propose the effectiveness of the mucociliary clearance that reduces the concentration of viral particles in the trachea by 2.6 times in 1 hour.

The number of bacteriophages in the lungs was higher than in the trachea. However, statistically significant reduce of the bacteriophage was not observed (see Table 2). According to the experimental model, no more than 3837 viral particles per hour can be eliminated from one lung via mucociliary clearance of the bronchial airway. The possible rate of the virus elimination for the lungs was no more than 1,21% of the detected number of viral particles in the lungs per hour.

Table 2. Concentrations of bacteriophage MS2 (Log₁₀ PFU/ml) in lungs, esophagus and trachea of mice post 1 and 2.5 hours of the inoculation onset.

The duration of the experiment	1h			2h 30 min		
	Lung	Trachea	Esophagus	Lung	Trachea	Esophagus
M \pm SD	5,502 \pm 0,403	4,282 \pm 0,19	3,269 \pm 0,587	5,116 \pm 0,406	3,672 \pm 0,407	3,279 \pm 0,348
CV	7,33	4,58	17,957	7,941	11,083	10,62
m	0,1648	0,08	0,239	0,165	0,166	0,142
p-value (T-test)	0,064	0,0039	0,4842			

Furthermore, there is a trend of bacteriophage concentration reduction in the trachea by 0,61 Log₁₀ post 1.5 hours (p-value < 0.01), while the trend is not observed in the oesophagus. The latter creates prerequisites for long-term transport of viral particles from the nasopharynx to the esophagus after aerosol and/or airborne droplet infection.

The efficiency of the viral particles transport from the intestines to the lungs

According to the experimental results, the appearance of Ph57 bacteriophage (Fig 3 a, b) in the lungs was observed within an hour post-onset intragastric administration of the bacteriophage. More than 6000 bacteriophage particles were found in the gastrointestinal tract of the experimental mice 1 hour later. Up to 3.65% of the bacteriophage (out of 7001 phage particles surviving after passing through the stomach) was detected in the lungs of mice with normal mucosal permeability. Thus, the ratio of bacteriophage numbers in the lungs to ones in the gastrointestinal tract was $1:256.08 \pm 168$ ($M \pm SD$) for an hour.

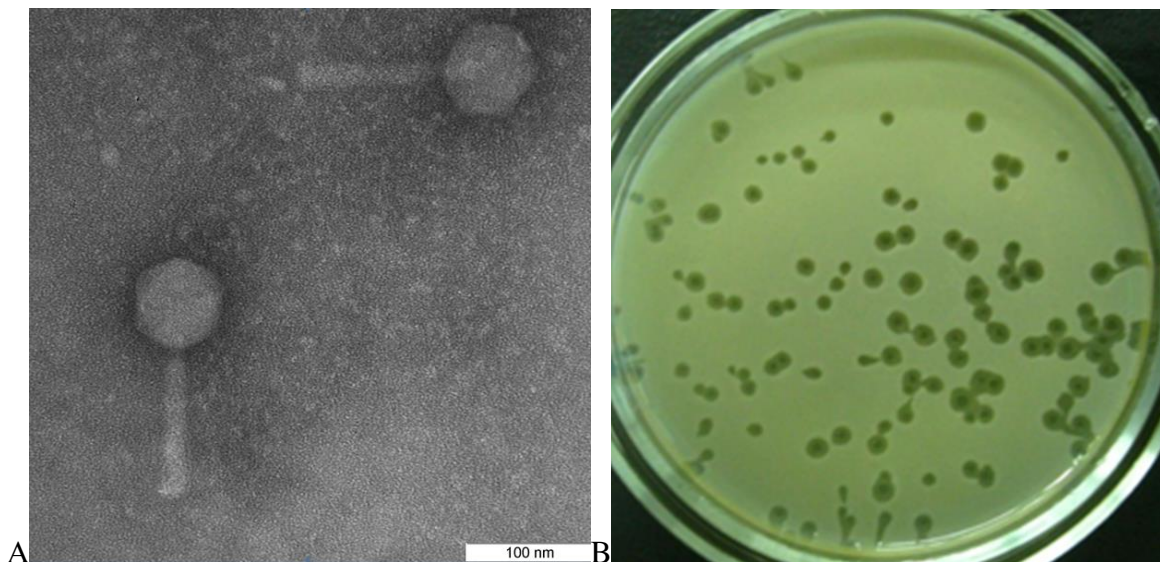


Fig. 3 An electron micrograph of a bacteriophage Ph 57 particle. Uranyl acetate staining method (a) and morphology of negative colonies of bacteriophage Ph 57 on a matte background of *P. aeruginosa* CEMTK 670 culture (b).

Model simulations of SARS-CoV-2 viral dynamics and distribution of the viral particles in different human organs and tissues

The main factor limiting the multiplication of the virus in each of the compartments is a decrease in a certain proportion of susceptible cells during the infection. At the initial stage of the infectious process, the penetration of the virus into a cell with an ACE2 receptor and a TMPRSS2 protease implies the formation of an appropriate amount of viral particles per unit of time. As the proportion of infected cells increases, the risk of entering an already infected cell proportionally increases. Of course, in this situation, an additional amount of viral particles can no longer be formed. Self-purification of the analyzed compartments due to the processes of renewal and degradation in this model does not change over time, but the effects of this process are summed up with a decrease in the efficiency of cell infection. The original data on the efficiency of the viral particles transport considering experimental bacteriophage models enables us to assume a more significant effect of the transport processes on the viral titer in lungs.

Based on the developed model and parameter values (Table 1), we conducted *in silico* experiments to investigate: 1) the effect of the transport processes on the viral load in each of the compartments; 2) the effect of an initial number of viruses infecting the epithelial cells of the nasopharynx, and 3) considering promoting cytotoxicity as an additional antiviral mechanism mediated by cytotoxic T lymphocytes and natural killer

cells (T-cellular response). In the first two cases, the basic antiviral mechanism was blocking *de novo* infection induced by neutralizing antibodies (B-cellular response) in different days post-infection depending on the compartment (see Table 1).

According to the model simulation results, the change in values of transport parameters from the nasopharyngeal region to the lung and from the intestine to the lung can significantly alter the trajectory of the viral load in all compartments (Fig. 4). Higher transport efficacy results in better outcomes of the disease suggesting complete viral clearance in the nasopharynx and the intestine on 15 and 30 days post-infection respectively. Moreover, the model also predicts the significant decline of the viral load in the lung under higher transport efficacy at the same time frame, while lower transport efficacy leads to the time shift of the peak viral load and more prolonged virus reproduction in the lung.

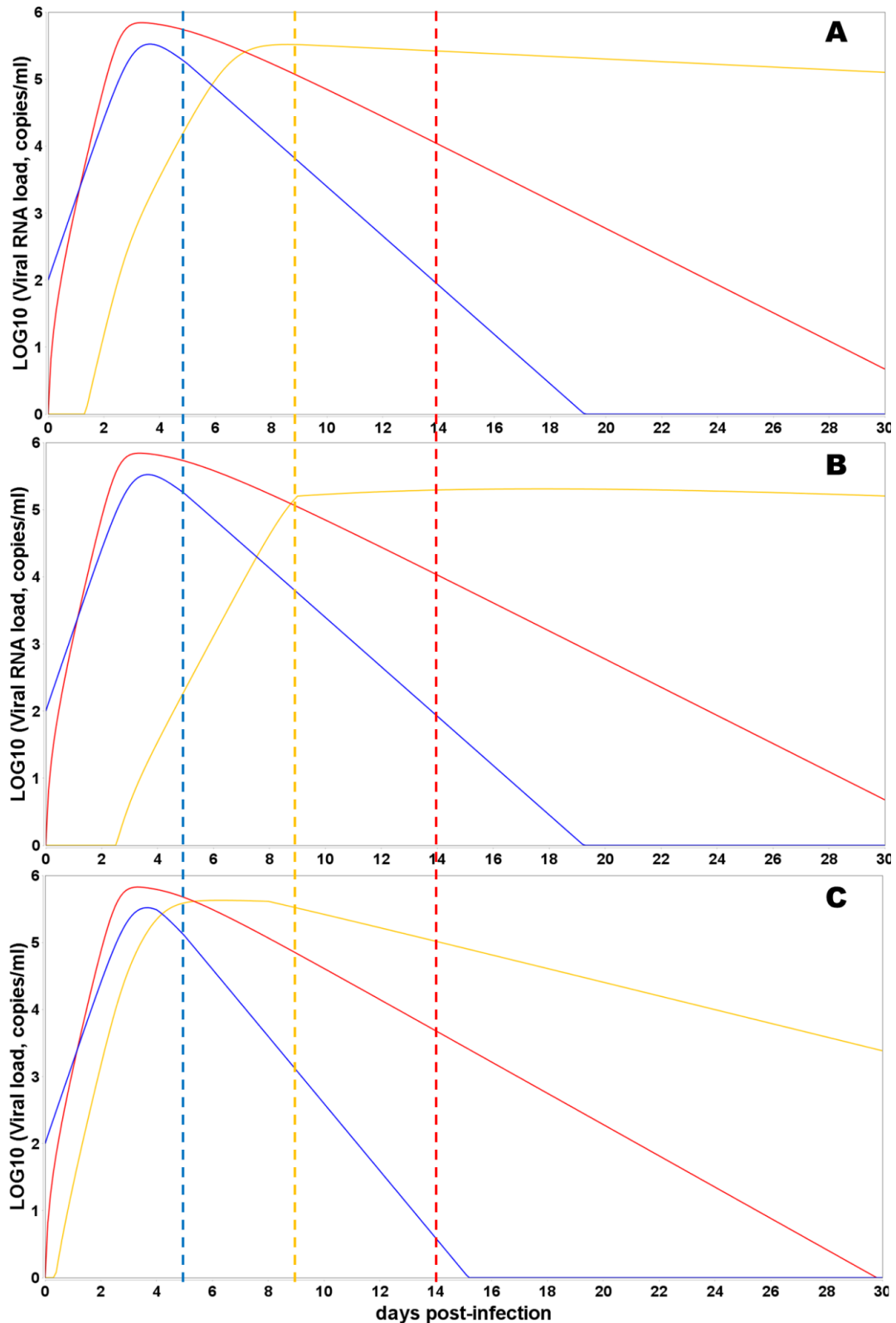


Fig. 4. Predicted viral load trajectories in the nasopharyngeal region (NP, blue curve), gastrointestinal tract (Intestine, red curve) and lungs (Lung, orange curve) are shown. The dashed vertical lines correspond to the timing of humoral immune response initiation in a certain compartment (the colour of the dotted line corresponds to the colour of the viral trajectory in the compartment). The initial viral load is 100 viral particles in the NP. Y-axis - log10 of viral load (copies/ml), X-axis - days from the moment of infection. A) values of the transport parameters correspond to the default

values from Table 1; B) values of the transport parameters from the nasopharyngeal region to the lungs and from the intestine to the lung were reduced 100 times; C) values of the transport parameters from the nasopharyngeal region to the lungs and from the intestine to the lung were increased 100 times.

The dose of infection, or the efficiency of accumulation of viral particles at the gate of infection, according to the results of mathematical modeling, should have a nonlinear effect on further development of the infectious process. A small dose of infection increases the length of the incubation period (Fig. 5a) and creates the prospects for the appearance of class A immunoglobulins on the mucous membranes with a minimum amount of virus entering the lungs through the circulatory system. At the same time, the immune response formed in the intestine will outpace the response of the immune system in the lungs by two days, which can potentially lead to suppression of the immune response in the lungs and the development of an asymptomatic form of pneumonia (but with a limited viral load at the initial stage). An increase in the infection dose by a factor of 1000 (Fig.5c) leads to synchronization of the accumulation of the virus in the nasopharynx and intestines and a higher total dose of virus accumulation in the lungs (which is estimated as the area under the curve (AUC)) at the time of the formation of a specific immune response and, accordingly, a more extensive inflammatory process.

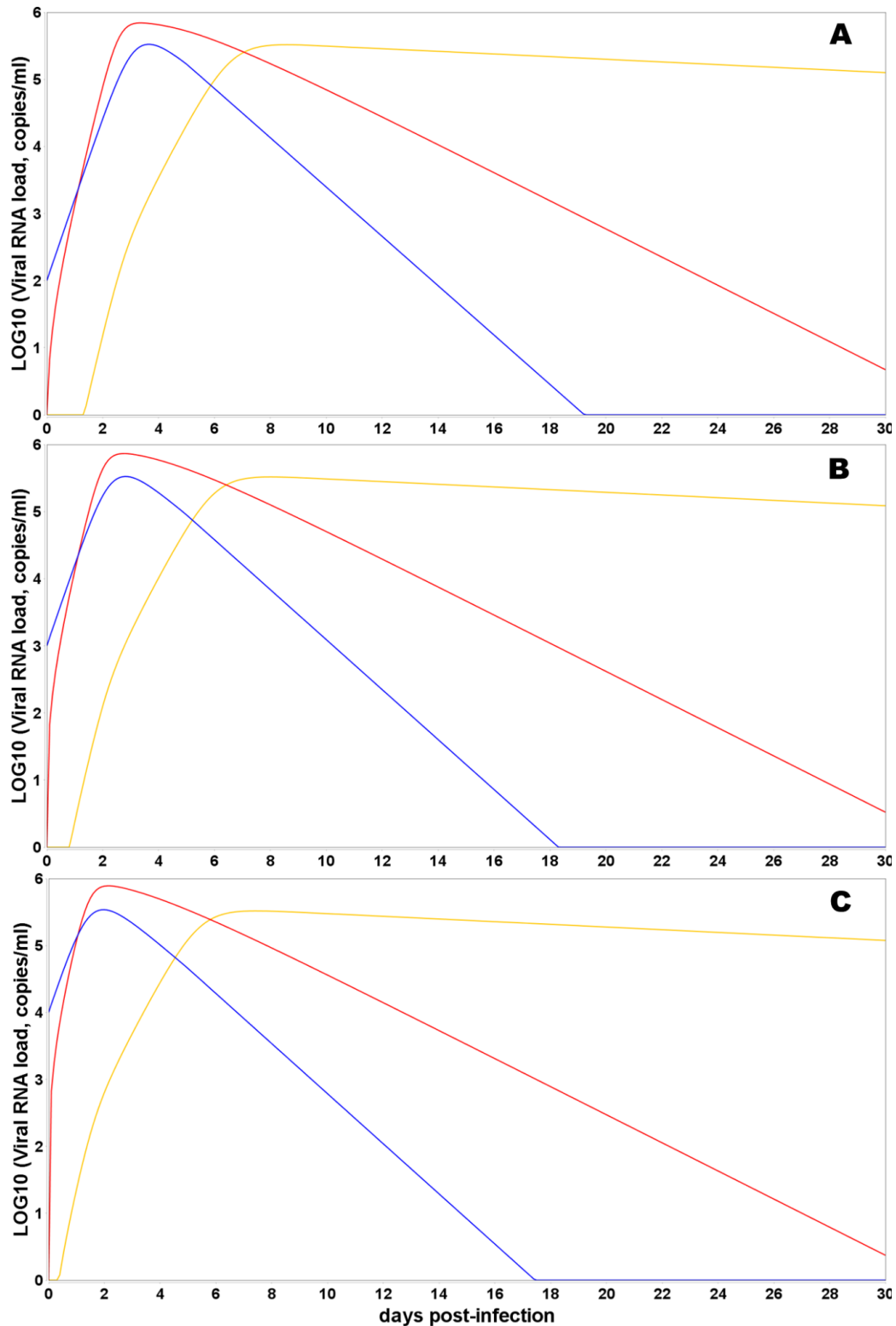


Fig. 5. Predicted viral load trajectories in the nasopharyngeal region (NP, blue curve), gastrointestinal tract (Intestine, red curve) and lungs (Lung, orange curve) are shown. The time of humoral immune response initiation in each compartment is the same as in Figure 3. The initial viral load is varied in the NP. Y-axis - log₁₀ of viral load (copies/ml), X-axis - days from the moment of infection. A) the initial dose of the viral particles corresponds to 10^2 ; B) the initial dose is 10^3 and C) the initial dose is 10^4 .

Eventually, we simulate the effect of combining cellular and humoral immune responses blocking *de novo* infection and promoting cytotoxicity (Figure 6). The combining effect of responses results in more rapid decay in viral load in all compartments. Moreover, the immune response mediated by cytotoxic T lymphocytes and natural killer cells and initiated after the viral load peak in each compartment can still reduce the AUC implying the crucial and most prominent effect of the T-cellular immune response in the viral clearance.

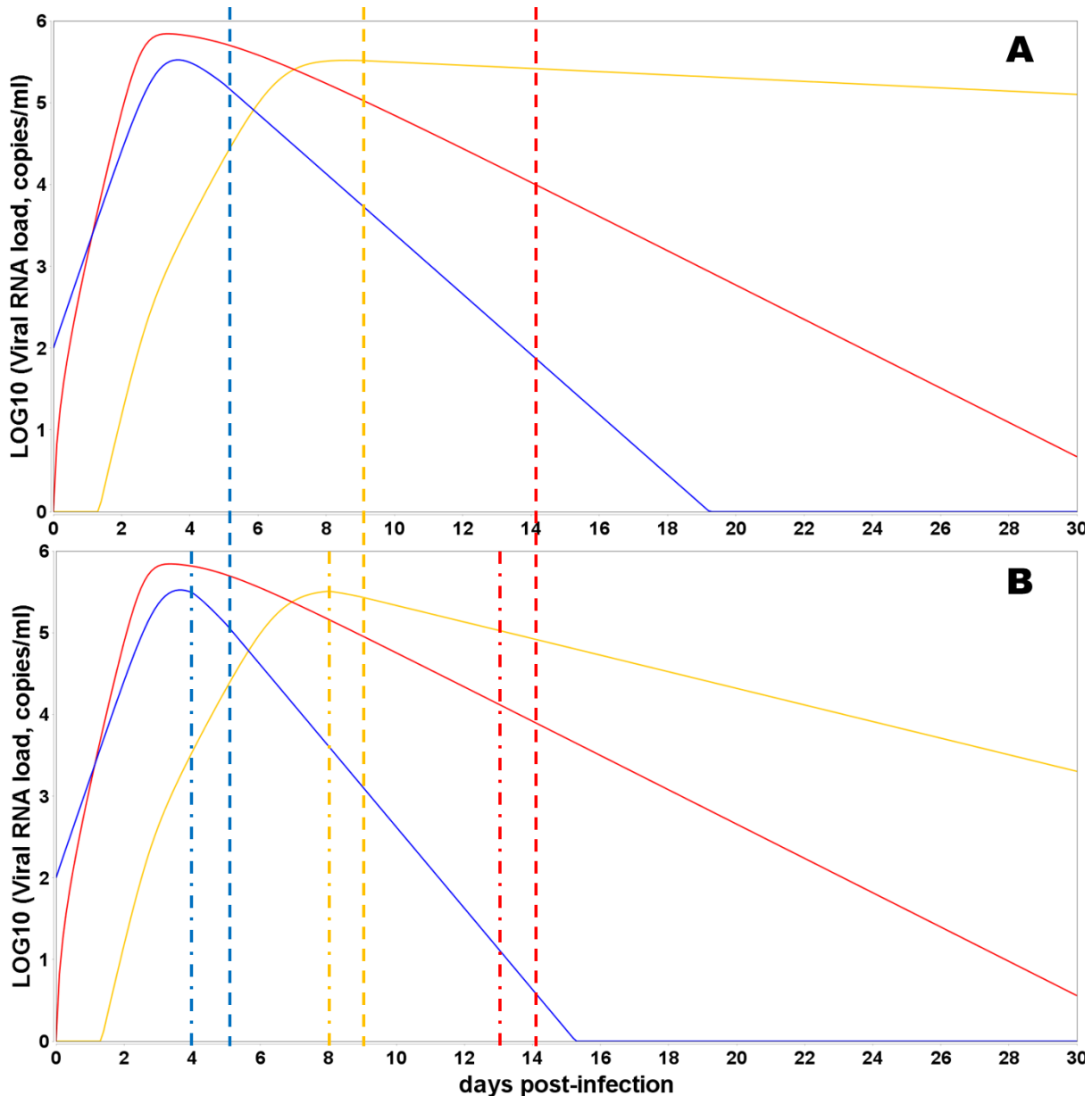


Figure 6. Predicted viral load trajectories in the nasopharyngeal region (NP, blue curve), gastrointestinal tract (Intestine, red curve) and lungs (Lung, orange curve) depending on the consideration of the T-cellular response are shown. The dashed vertical lines correspond to the timing of humoral immune response initiation in a certain compartment, while dash-dotted lines represent the initiation of T-cellular immune response in a certain (the colour of the dashed and dash-dotted lines correspond to the colour of the viral trajectory in the compartment) The initial viral load is 100 viral particles in the NP. Y-axis - log10 of viral load (copies/ml), X-axis - days from the moment of infection. A) only B-cellular response is involved in the virus clearance; B) B- and T-cellular responses are activated.

Sensitivity analysis of the model

Using sensitivity analysis we have determined to which model parameters the uninfected target cell proportion in each compartment is more sensitive. Such analysis tells us the importance of each parameter on the infectious process in the corresponding compartment. Figure 7 presents results of the analysis and demonstrates sensitivity indices of the model with respect to f_i in a certain module. From the figure it is clear that the variable is the most sensitive to the maximum rate constant for viral replication, γ_{nf} . It indicates that an increase in the parameter value will be followed by an immediate decrease in the proportion of uninfected target cells. Moreover, the variable is significantly sensitive to the transport rate constant, $K_{tr_{nfI}}$, meaning that faster transport of the virus from the nasopharynx to the intestine can lead to more target cells in the former remain uninfected. It is also intriguing that the proportion of uninfected target cells in the compartment is sensitive to the time frame of the humoral response initiation in the nasopharynx. The obtained result suggests a strategy to control the initial stage of the infection in an organism via a drug improving humoral response initiation in the nasopharynx.

The fraction of target cells that remain uninfected in the intestine, in turn, is the most sensitive to the death rate of infected cells (and viral particles in these intestine cells, respectively), δ_I . It indicates that renewal processes of the intestinal mucosa may play an essential role in the infection dynamics in the intestine. The interesting aspect of the analysis for the compartment is the sensitivity of the intestinal fraction to the SARS-CoV-2 life cycle in the nasopharynx (infection and replication rate constants, β_{nf} and γ_{nf} , as well as the death rate, δ_{nf}). The result also confirms potential benefit of an infection control strategy via the gate of infection, nasopharynx. Eventually, the fraction of uninfected lung cells is also sensitive to the virus replication in the compartment, γ_{\square} , but the variable in the lung is mostly sensitive to the effectiveness of the humoral response, ϵL , blocking *de novo* infection and time frame of the response, $time_{\epsilon L}$. So, the infection dynamics in the lung is mainly determined by the humoral immune response and its onset proposing the treatment way in combating SARS-CoV-2 in human lungs.

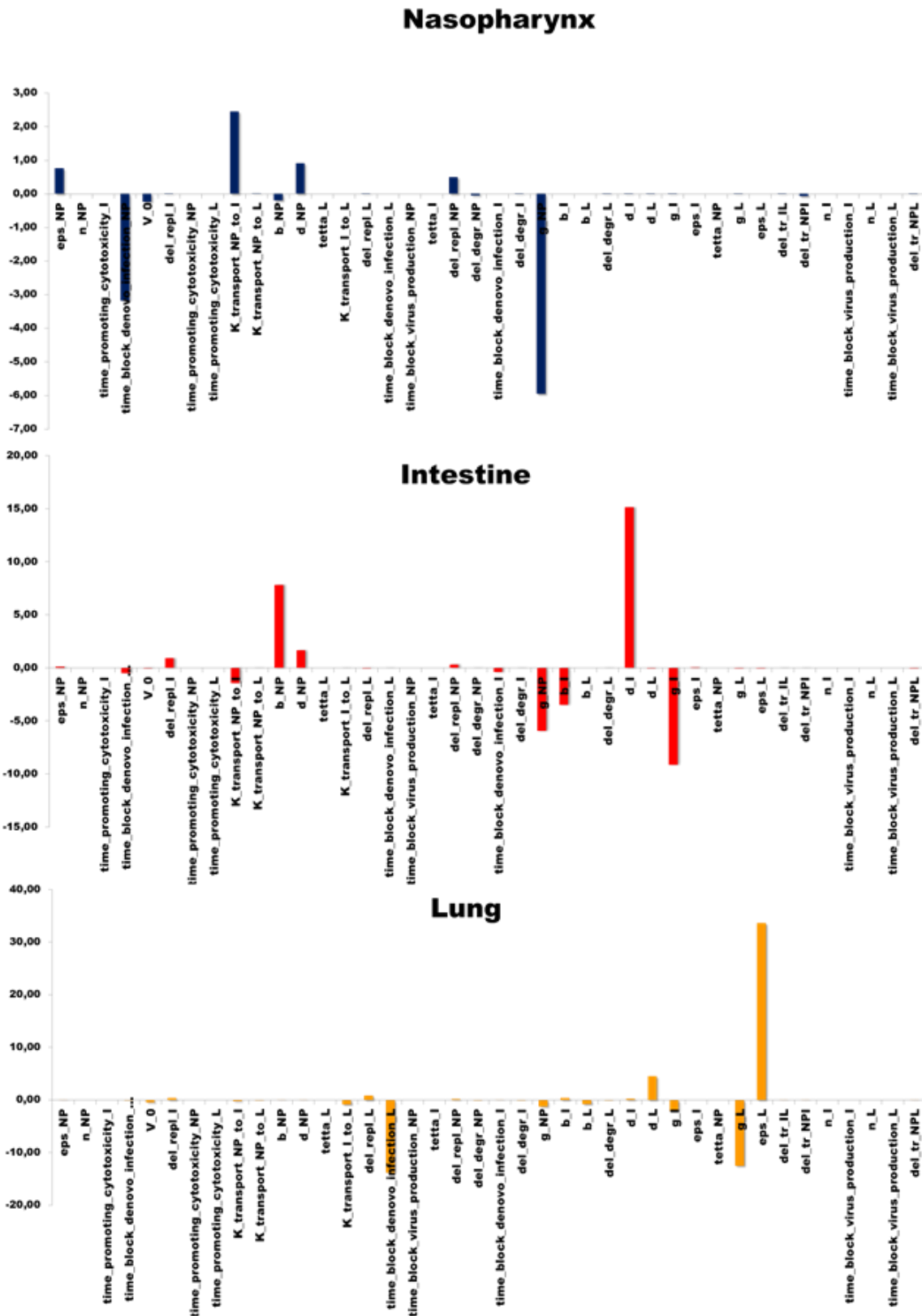


Fig. 7. Sensitivity analysis of the model. The target variables in the analysis correspond to the target cell ratios in each compartment, where the column height indicates the scaled sensitivity's value of the variable to a certain model parameter.

Sanitation of the intestines and nasopharynx with virucidal drugs

The results of the model simulation of the sanitation with virucidal medicines of the nasopharynx only (Case 1) and of both the nasopharynx and intestines (Case 2) are summarized in the Table 3. It is shown that the sanitations significantly decrease the viral load in corresponding compartment. However, there is no statistically significant decline of the viral load in the lungs in both cases.

Table 3. The viral peak load and day post-infection during the suppression of virus accumulation in the nasopharynx only (Case 1) and in both compartments (Case 2).

Dose of the infection, Log10 PFU	Control			Case 1			Case 2		
	Nasopharynx	Intestine	Lungs	Nasopharynx	Intestine	Lungs	Nasopharynx	Intestine	Lungs
1,69	5,5	5,75	4,75	3,7	5,7	4,7	3,7	5,5	4,25
2	5,5	5,8	4,8	3,2	5,8	4,75	4	5,5	4,35
2,69	5,5	5,8	4,85	4,8	5,85	4,8	4,6	5,7	4,7
3	5,5	5,8	4,9	4,25	5,85	4,8	4,7	5,75	4,8
3,69	5,51	5,8	5	4,8	5,85	4,8	4,7	4,7	4,8
M	5,502	5,79	4,86	4,15	5,81	4,77	4,34	5,43	4,58
SD	0,004	0,022	0,096	0,700	0,065	0,045	0,462	0,424	0,261
p-value (T-test: Case1 vs Control)	0,00128	0,26730	0,04717						
p-value (T-test: Case2 vs Control)	0,00025	0,04717	0,02733						

Note: in the experiment, $\gamma_{\square} = 1.0$; epsilon = 0.995, one day after the onset of infection; SD - standard deviation; M - medium.

Discussion

Presented results of the model analysis and conducted experiments with bacteriophages biodistribution drive us to formulate the next scheme of the COVID-19 pathogenesis in humans.

Airborne infection involves the predominant entry of SARS-CoV-2 viral particles into the nasopharyngeal region of the upper respiratory tract, followed by reproduction and transport of viral particles into the esophagus. The viral particles that have entered into the trachea and bronchi will be eliminated from the trachea to the oral cavity and transfer to the gastrointestinal tract, but not into the lungs as follows from the experiment with viral particles that are not capable to replicate in cells of the mice (Table 2). Furthermore, experimental results on the bacteriophages [20] biodistribution demonstrates a rapid decrease in the concentration of bacteriophage by 4 times in the tracheal mucosa. This outcome can be explained by a combination of two factors: 1 - cessation of the entry of new portions of viral particles with aerosol into the trachea, 2 - active elimination of viral particles from the trachea into the nasopharynx and esophagus.

The amount of bacteriophage in the lungs, on average, statistically insignificantly decreased by 2.5 times at the same time frame that can be potentially explained by the both passive sorption and phagocytosis of antigenically distinct particles. Considering this experiment as a model of COVID-19 to infect the bronchi by the viral particles, the viruses must increase their numbers 3 times per hour (on average) to ensure reproduction and further dissemination along the bronchial tree to the lungs [21]. The result does not contradict the published data [22]. The entry of viral particles into the lungs with an aerosol significantly reduces the requirements for the rate of virus reproduction due to a significantly lower rate of renewal of respiratory epithelial cells [11].

We also believe that any infection transmitted by airborne droplets will be accompanied by the entry of a significant part of the viral particles into the gastrointestinal tract. The resistance of viral agents to gastric juice will determine the likelihood of cells infection in the gastrointestinal tract. The published data has already shown the high resistance of SARS-CoV-2 to the acidic environment of the stomach [16].

Another important factor is the low efficiency of reproduction of the SARS-CoV-2 virus in the bronchi and trachea. This fact, in our opinion, determines the large contribution of the transport processes of viral particles from the compartments of the body with high synthetic efficiency and secretion of proteins (including viral ones) to the compartment in which the efficiency of regeneration of damaged cells is low, i.e. into the lungs.

The mucous membrane in the area of the nose and nasal sinuses occupies as follows from the simulation results, the concentration of viral particles in 1 ml of nasopharyngeal fluid reaches 5.5 Log₁₀ viral particles per 1 ml (Figures 4, 5). In general, this does not contradict the published data. The SARS-CoV-2 virus was detected in saliva at concentrations of 10⁴-10⁸ RNA copies per 1 ml of saliva [23]; the average saliva production in an adult is 1-1.5 liters per day [24].

Based on these data, we can calculate that with the participation of the salivary glands and goblet cells producing mucin in the stratified non-keratinizing epithelium of the oral cavity, up to 10⁷-10¹¹ viral particles should be formed per day, most of which should enter the esophagus and/or enter the contact with immunocompetent cells of the nasopharyngeal region. The average daily volume of mucus produced by the bronchi and tracheal mucosa ranges from 10 to 100 ml [25]; the concentration of the virus in the broncho-

alveolar lavage can fluctuate between 2×10^6 - 2.6×10^8 copies of viral RNA in 1 ml, that is, the daily isolation of the virus can reach values of 10^9 - 10^{10} copies of viral RNA, provided there is a significant proportion of bronchi infected with the virus. Experiments with organ cultures show that the concentration of viral particles in 1 ml of culture fluid can be 10^{10} copies of viral RNA [6, 10], and these values are clearly lower than those obtained when testing swabs.

ies an area of 120-200 cm^2 [21, 26], up to 15% of cells can be occupied by Goblet cells [7, 26], including those capable of producing SARS-CoV-2 [4] and mucin. The total production of mucus by the upper respiratory tract is up to 2 liters, which provide mucociliary clearance, in the process of passing through the upper respiratory tract $\sim 12 \text{ m}^3$ of air per day [7, 24]. If we subtract from the total volume of mucus, mucus from the trachea and saliva, then we can assume the production of ~ 400 -500 ml of fluid by the nasopharyngeal region per day. Most of the mucus, apparently, dries up, moistening the incoming air, and part of the mucus from the deep parts of the nasal sinuses also flows down to the pharynx, contacting with tonsils. At the initial phase of the infectious process (4-5 days from the onset of symptoms), the concentration of the virus in the nasopharyngeal region can reach 10^8 copies of viral RNA per 1 ml [27], which should correspond to the daily production of the virus in the amount of $\sim 10^{10}$ - 10^{11} copies of viral RNA.

Since the bulk of the broncho-tracheal, nasal mucus and saliva, together with $\sim 10^{11}$ copies of the virus, for a long time, enters the esophagus, it can be confidently stated that after the development of a local infectious process in the nasopharyngeal region, subsequent infection should affect the gastrointestinal mucosa, not the lungs. Dynamics of the accumulation of SARS-CoV-2 in the lungs and nasopharynx, in general, reflects this assumption (Figure 4). As follows from the proposed model (Figure 4), a lower efficiency of virus transport from the nasopharyngeal region and intestine (through the circulatory system) to the lungs compared to the transmission of the virus from the nasopharynx and oral cavity to the intestine (with saliva and mucus) is evident. In this case, the anticipatory accumulation of SARS-CoV-2 in the intestine relative to the lungs does not contradict the observed clinical picture: the onset of symptoms of intestinal upset before the onset of clinical signs of pneumonia [28, 29].

Entering the gastrointestinal tract of viral particles in an amount equivalent to $\sim 10^{10}$ - 10^{11} copies of viral RNA will obviously be accompanied by infection of the intestinal epithelium and accumulation of the virus in the intestinal lumen in an amount proportional to the number of cells susceptible to the infection, multiplied by their secretory and protein-synthetic activity. Similar mechanisms of cross-infection of both the intestine and the lungs have been described, for example, in rhinovirus infection, coronavirus OC43 infection [30].

A very large area of the mucous membrane of the gastrointestinal tract (~ 100 -300 m^2), combined with a high activity of protein synthesis, cell division (which should contribute to the formation of large

amounts of viral particles), with a very high rate of mucosal renewal (48-72 hours) and elimination contents of the gastrointestinal tract. In comparison with the gastrointestinal tract, in the lungs, the respiratory epithelium is renewed approximately every 22-35 days [11]. It results in lower rate of the protein synthesis in the tissue. At the same time, the histological structure of the alveoli implies the rate of purification of their contents, comparable to the rate of synthesis of biopolymers and desquamation of cells of the respiratory epithelium into the lumen of the alveoli.

Thus, the most obvious presence of a local infection phase, accompanied by long-term localization of SARS-CoV-2 viral particles on the mucous membranes of the nasopharyngeal region and/or intestine, but not in the lungs, where antigen presentation should be accompanied by the formation of IgG.

As follows from our model, the concentration of the virus in the lungs increases more slowly than in the intestine and nasopharynx (Figure 4-6). It is noteworthy that the maximum amount of virus in the lungs is 5-10 times less (due to the lower anabolic activity of the respiratory epithelium and the endothelium of the blood vessels of the lungs). On the other hand, in our model, the concentration of SARS-CoV-2 in the lungs remains at a consistently high level for longer than in the nasopharynx and intestines. This fact is due to the lower rate of lung self-renewal.

The analysis of research published data and conducted model simulation have prompted us to pose the question: is the presence of SARS-CoV-2 in the lungs a consequence of hematogenous transport of the viral particles from the intestine, or is it mainly the result of independent reproduction of the virus in the lung tissue?

The presence of a viral agent in the gastrointestinal tract is an established fact [31-33]. Long-term persistence of the virus in the intestine [33] is possible only when the virus reproduction rate is comparable to the rate of renewal of the intestinal contents. The earliest signs of COVID-19, accompanied by nausea and sometimes diarrhea [31-32], are also possible if the viral agent enters the intestines earlier than the lungs [31, 34]. The very fact of the presence of the virus in samples of intestinal contents is not associated with the severity of the damage to the respiratory system [33, 34]. It should be borne in mind that the most likely accumulation of the viral agent in the small intestine, therefore, signs of diarrhea (detected, on average in 50.5% of cases [32]) maybe absent due to the absorption of exudate formed in the small intestine. For the same reason, it is possible to reduce the number of viral particles and the copy number of viral RNA (detected in 48.1% of cases [35] under the action of enzymes (proteases, RNases and lipases), including those of bacterial origin. Accordingly, the accelerated passage of food masses through the intestine should increase the likelihood of detecting viral RNA by PCR in the presence of diarrheal syndrome [35]. The copy number of SARS-CoV-2 genomic RNA in stool samples ranges from 1×10^2 to 1×10^8 copies/ml [36] depending on the presence of the diarrhea, respectively. If we estimate the volume of daily excretion of intestinal contents

with a mild form of diarrheal syndrome > 700 ml / d, then the daily production of the virus should exceed 7×10^{11} copies.

The concentration of viral RNA and viral particles in experiments with transplanted cell cultures is 9.6×10^6 and 5.2×10^3 [27]. Most likely, PCR of intestinal contents gives underestimated amounts of RNA compared to the results of PCR testing of the upper respiratory tract, due to the accelerated degradation of viral RNA by intestinal RNases. For the same reason, when modeling, one should consider the number of viral particles, which are underestimated by three orders of magnitude, relative to the literature data, with the exception of the intestine (this is due to the high rate of degradation of RNA molecules in the intestine).

Experiments with transplantable cultures of human intestinal cells *in vitro* show the production of the virus $2-8 \times 10^7$ GE/ml, that corresponds to the production of 3.5×10^6 GE / ml per day. If we recalculate the production of the virus per $200-300$ m² of the mucosal area, then the production of the virus should be up to 4.2×10^{11} GE/day. It is worth to note that estimates of the gut viral production based on different data sources differ by three orders of magnitude. However, long-term persistence of the virus in the intestine [37], lasting up to 5 weeks, implies the rate of viral reproduction, limited by the rate of renewal of the intestinal mucosa. It follows from this that a comparable amount of virus in the lungs can be provided only by a slow rate of elimination of viral particles from the alveoli, since the rate of renewal of the respiratory epithelium is lower than in the intestine, more than 10 times. In this regard, with a comparable efficiency of the transport of viral particles into the efferent blood vessels and lymphatic pathways in the lungs and intestines, one can argue about at least 10 fold more active intake of viral agents from the blood into the lungs than the spread of viral particles with blood from the lungs along the large circle of blood circulation to all organs. Consequently, an intense contact of the viral agent occurs earlier with the intestinal immune system, and not the lungs. For this reason, our model is characterized by: 1) primary infection of the nasopharyngeal region (gate of infection) and 2) higher rate of transport of the viral particles from the nasopharyngeal region to the intestine compared to the transport rate of the particles from the intestine and nasopharyngeal region to the lungs.

Furthermore, we have also simulated the adaptive immune responses. The time onset of the immune response differs in modeled compartments. Firstly, immunocompetent cells recognizing SARS-CoV-2 antigens produce in the nasopharynx and regional lymph nodes. Due to the fact that the accumulation rate of immunocompetent cells obeys a power-law function, the lymphatic system of the nasopharynx that will be the primary source of Th2 CD4+ T lymphocytes for both the respiratory system and the whole organism. As viral particles enter the intestines and lungs, differentiation and proliferation of T- and B- lymphocytes in the lungs and lymph nodes of the lungs, bronchi, and mediastinum should be expected. In our model, we consider the formation of adaptive immune response in the lungs the 9th day post- infection. The time onset of local antiviral reactions of the adaptive immunity in the intestine is supposed to be at 14 days post infection, after

the formation of a systemic immune response or the migration of a critical mass of the lymphocytes from the lungs and nasopharynx to the intestine (Table 1).

In this model, the formation of an immune response is limited to 5 days separately for the studied compartments and implies the death of infected cells. Since the primary infection and accumulation of SARS-CoV-2 occurs in the nasopharyngeal region, it seems clear that the primary immune response is generated in the nasopharyngeal region.

Since initially all antigen-specific T-lymphocytes passing through the afferent lymphatic ducts pass through the pulmonary circulation, their influence on the formation of an adaptive immune response in the lungs should be considered maximum, and in the intestine - minimum. For this reason, the immune system of the nasopharyngeal region and regional lymph nodes, as we assume, is the most important element in the formation of an immune response both at the initial stage of infection and at the stage of development of viral lung damage. Since the pathology of the lungs is associated with the damaging effect of cells of the immune system (lymphocytes, macrophages and neutrophils) - the nasopharynx is the most important source of these cells [38, 39].

The applied significance of our model is the need for local therapy of a viral infection, in compartments with a potential maximum rate of reproduction of viral particles, at least at the initial stage of the infectious process [Table No. 3].

The created model implies a relatively low intensity of the spread of the virus through the lung tissue, considering the nasopharynx and intestines as the main sources of the viral agent in the body, incl. and for the respiratory system. Therefore, a decrease in the viral load only in the nasopharynx or only in the intestine is not able to affect the viral load in the lungs, but should significantly change the nature of immunological reactions in the lungs, at the initial stages of the infectious process. However, the nature of the formation of the immune response in these compartments can be diametrically opposite (proliferation and transport of T-suppressors and T-helpers, respectively), therefore, the order of reaching peak concentrations of SARS-CoV-2 (depending on local immunoreactivity, mucosal integrity, efficiency transport SARS-CoV-2, the dose of infection) in the nasopharynx and intestines theoretically can be the main factor causing the development of immune-mediated damage of the vessels and respiratory epithelium of the lungs, or the asymptomatic course of COVID-19.

An important factor in our model that limits the reproduction of a viral agent in body tissues is the specific proportion of sensitive cells (f_i). Obviously, under the real conditions of a living organism, the death of the organism will occur before the amount of f_i is reduced to values that limit the reproduction of the virus. In any case, this may concern the vascular endothelium and the respiratory epithelium. Accordingly, the ratio

of the virus replication rate γ_i and the rate of degradation of viral particles δ_i is not at the equilibrium point, in our model. For this reason, a shift in the dynamics of virus accumulation in the body under the influence of adaptive immunity reactions becomes possible only at values of θ and $\epsilon \sim 1.0$. This feature of the model brings it closer to modeling a viral infection and the antiviral effect of antibodies in cell culture. A closed cell culture system also makes it possible to suppress a viral infection only with 100% inactivation of viral particles by virus-neutralizing antibodies. It is obvious that the very fact of the constant elimination of viral particles in the body (washing out of viral particles from the mucous membranes, destruction under the action of enzymes, etc.) should significantly increase the effectiveness of the sanitation of the mucous membranes from the virus both with drugs and antibodies.

As follows from the data the effect of virucidal substances [40-44] on coronaviruses in the intestinal lumen [40, 41] was accompanied by a decrease in the intensity of lung damage [40]. These facts show the importance of reducing the hematogenous transport of viral particles from the intestinal lumen to the lungs.

The simulation results allow us to state that the sanitation of the mucous membranes of the nasopharynx of the gastrointestinal tract at the initial stage of the infectious process, with the participation of adaptive immunity reactions, has prospects for use in medical practice.

Conclusion: Comparison of the published data on SARS-CoV-2 concentration in the lungs, nasopharynx and intestines with the mass of these organs and the intensity of synthetic processes in mucosal cells suggests that the relatively high concentration of this virus in the lungs is not due to intensive reproduction of viral particles. It is rather enabled by slower process of their destruction / elimination in the lungs compared to the nasopharynx and intestines. The relatively low concentration of SARS-CoV-2 in tissues implies an essential role of the transport processes and redistribution of the virus in the body from the compartments with intensive reproduction of the virus (nasopharynx and intestines) to organs and systems, where the entry of the virus can create life-threatening conditions (lungs). The results of the model simulations show that the intestine and nasopharynx, as a source of SARS-CoV-2 for the lungs, are equivalent.

Acknowledgments

The study was supported financially by the RFBR (#20-04-60355 “Development of a multi-scale immuno-epidemiological mathematical model COVID-19, taking into account the impact on the economy of the region and the scenarios of authority actions”

References

1. Huang, C. et al. Clinical features of patients infected with 2019 novel coronavirus in Wuhan, China. *Lancet*, 2020, 395, 497–506.
2. Guan Wei-Jie; Ni Zheng-Yi; Hu Yu, Liang Wen-Hua; Ou Chun-Quan; He Jian-Xing; Liu Lei. Clinical characteristics of coronavirus disease 2019 in China. *N. Engl. J. Med.* 2020, doi: 10.1056/NEJMoa2002032. February
3. Woelfel R; Corman VM; Guggemos W; Seilmaier M; Zange S; Mueller MA; et al. Virological assessment of hospitalized cases of coronavirus disease 2019. *Nature*. 2020, (2020.03.05.20030502)
4. Sungnak; W.; Huang; N., Bécavin, C.; Berg, M. and HCA Lung Biological Network. SARS-CoV-2 entry genes are most highly expressed in nasal goblet and ciliated cells within human airways. *ArXiv* 2020, arXiv:2003.06122v1. Available online: <https://arxiv.org/abs/2003.06122> (accessed on 13 Mar 2020).
5. Schaefer I.M.; Padera, R.F.; Solomon, I.H. et al. In situ detection of SARS-CoV-2 in lungs and airways of patients with COVID-19. *Mod. Pathol.* 2020, 33, 2104–2114 <https://doi.org/10.1038/s41379-020-0595-z>
6. Zheng S.; Fan J.; Yu F.; Feng B.; Lou B.; Zou Q.; et al., Viral load dynamics and disease severity in patients infected with SARS-CoV-2 in Zhejiang province, China, January–March 2020: retrospective cohort study. *BMJ*. 2020, 369: m1443
7. Cole P. Nasal and oral airflow resistors. Site, function, and assessment. *Arch Otolaryngol Head Neck Surg*. 1992, 118, 8, 790-793.
8. Kolpakov, F.; Akberdin, I.; Kashapov; T.; Kiselev, L.; Kolmykov, S.; Kondrakhin, Y.; Kutumova, E.; Mandrik, N.; Pintus, S., Ryabova; A. and Sharipov, R., . BioUML: an integrated environment for systems biology and collaborative analysis of biomedical data. *Nucleic acids research*, 2019, 47, W225-W233.
9. Akberdin, I. R.; Kiselev, I. N.; Pintus, S. S.; Sharipov, R. N.; Vertyshev, A. Y.; Vinogradova, O. L.; Popov, D. V.; Kolpakov, F. A., A modular mathematical model of exercise-induced changes in metabolism, signaling, and gene expression in human skeletal muscle *International Journal of Molecular Sciences*. 2021, 22, 19, 10353.
10. Kim, K.S.; Ejima; K., Iwanami, S.; Fujita, Y.; Ohashi, H.; Koizumi, Y.; Asai, Y.; Nakaoka, S.; Watashi, K.; Aihara, K. and Thompson, R.N.; 2021. A quantitative model used to compare within-host SARS-CoV-2; MERS-CoV, and SARS-CoV dynamics provides insights into the pathogenesis and treatment of SARS-CoV-2. *PLoS biology*, 19, e3001128.
11. Bertalanffy F.D. - Respiratory tissue: structure, histophysiology, cytodynamics. Part II. New approaches and interpretations. *Tnt. Rev. Cytol.*, 1964, 17, 213- 297
12. Cheung Ka Shing; Hung Ivan F.N.; Chan Pierre P.Y.; Lung K.C.; Tso Eugene; Liu Raymond; Ng Y.Y. Gastrointestinal manifestations of SARS-CoV-2 infection and virus load in fecal samples from the Hong Kong cohort and systematic review and meta-analysis. *Gastroenterology*. 2020, doi: 10.1053/j.gastro.2020.03.065.
13. Wang, S.; Hao, M.; Pan, Z.; Lei, J.; Zou, X.; Data-driven multi-scale mathematical modeling of SARS-CoV-2 infection reveals heterogeneity among COVID-19 patients. *PLoS Comput Biol* 2021, 17, e1009587. <https://doi.org/10.1371/journal.pcbi.1009587>
14. Cao, W.; Chen, Y.; , Alkan, S.; Subramaniam, A.; Long, F.; Liu, H.; Diao, R.; Delohery, T.; McCormick, J; Chen, R; Ni, D; Wright, P.S.; Zhang, X.; Busch, S.; Zilberstein, A.; Human T helper (Th)

cell lineage commitment is not directly linked to the secretion of IFN-gamma or IL-4: characterization of Th cells isolated by FACS based on IFN-gamma and IL-4 secretion. *Eur J Immunol.* 2005, 35, 2709-2717. doi: 10.1002/eji.200425957. PMID: 16106470.

15. MacLennan, Ian C. M.; Gulbranson, Ju. A.; Toellner, K. M.; Palleja, C.; Sze, D. M.; Chan, E. Y.; Luther, S. A.; Orbea H. A. The changing preference of T and B cells for partners as T-dependent antibody responses develop. *Immunol Rev* 1997,156, 53–66.

16. Zhi-ping Sun; Xia Cai; Chen-jian Gu; Rong Zhang; Wen-dong Han; Yun Qian; Yu-yan Wang; Wei Xu; Yang Wu; Xunjia Cheng; Zheng-hong Yuan; You-hua Xie; Di Qu Stability of the COVID-19 virus under wet, dry and acidic conditions. *medRxiv* 2020.04.09.20058875; doi: <https://doi.org/10.1101/2020.04.09.20058875>

17. Rabitz, H.; Kramer, M.; and Dacol, D. Sensitivity analysis in chemical kinetics. *Annual review of physical chemistry*, 1983, 34, 419-461.

18. Davydova, N.V.; Koptev, V. Yu.; Kozlova, Yu. N.; Sulimova, L.I.; Afonyushkin, V.N.; Cherepushkina, V.S. Estimation of permeability to bacteriophages of intestinal mucosa of chickens with eimeriosis//*Siberian Herald of Agricultural Science* 2019, 49, 57-63 DOI:10.26898/0370-8799-2019-2-7

19. Kozlova, Iu.N., Repin,V.E.; Maiborodin, I.V. Treatment of the Surgical Infection Caused Pseudomonas Aeruginosa in Experiment //*Journal of Experimental and Clinical Surgery.* 2013, 6, 425-431 <https://vestnik-surgery.com/index.php/journal/article/view/227/185>

20. Turgeon, N.; Toulouse, M.J.; Martel, B.; Moineau, S.; Duchaine, C. Comparison of Five Bacteriophages as Models for Viral Aerosol Studies *ASM Journals Applied and Environmental Microbiology* 2014, 80, 42-50.

21. Mygind, N.; Pedersen, M.; Nielsen, M.; Morphology of the upper airway epithelium. In: *The Nose.* Proctor D, Andersen, I., Ed.; Amsterdam: Elsevier; 1982, pp. 71-97

22. Schaefer, I.M.; Padera, R.F.; Solomon, I.H. et al. In situ detection of SARS-CoV-2 in lungs and airways of patients with COVID-19. *Mod Pathol*, 2020, 33, 2104–2114. <https://doi.org/10.1038/s41379-020-0595-z>

23. Jialou, Zhu; Jiubiao, Guo; Yuzhong, Xu; and Xinchun, Chena Viral dynamics of SARS-CoV-2 in saliva from infected patients *J Infect.* 2020, vol. 81, no. 3: e48–e50. Published online 2020 Jun 25. doi: 10.1016/j.jinf.2020.06.0593.

24. Sue, P. Humphrey, Russell T. Williamson, A review of saliva: Normal composition, flow, and function // *Journal of prosthetic dentistry*, 2001, 85, 162-169, DOI:<https://doi.org/10.1067/mpr.2001.113778>

25. Toremalm, N.G. The daily amount of tracheobronchial secretions in man. *Acta Otolaryng* 1960, 158, 43-53.

26. Fomin, V. M.; Ganimedov, V. L.; Melnikov, M. N.; Muchnaya, M. I.; Sadovsky, A. S.; Shepelenko, V. I. Numerical simulation of air flow in the human nasal cavity with imitation of the clinical method of the anterior active rhinomanometry *Applied mechanics and technical physics.* 2012, 53, 8-66

27. Kenrie, P. Y. Hui; Man-Chun, Cheung; Ranawaka, A. P. M. Perera; Ka-Chun, Ng; Christine, H. T. Bui; John, C. W. Ho.; Mandy, M. T. Ng.; Denise, I. T. Kuok; Kendrick, C. Shih.; Sai-Wah, Tsao; Leo, L. M. Poon; Malik, Peiris; John, M. Nicholls; Michael, C. W. Chan Tropism, replication competence, and innate immune responses of the coronavirus SARS-CoV-2 in human respiratory tract and conjunctiva: an analysis in ex-vivo and in-vitro cultures// *The Lancet*, 2020, 8, 687-695

28. Gu, Jinyang; Han, Bing.; Wang, Jian COVID-19: gastrointestinal manifestations and potential fecal–oral transmission. *Gastroenterology.* 2020, doi: 10.1053/j.gastro.2020.02.054. March.

29. Wang, D.; et al. Clinical characteristics of 138 hospitalized patients with 2019 Novel Coronavirus-infected Pneumonia in Wuhan, China. *JAMA*, 2020, 323, 1061–1069
30. Openshaw, P.; Crossing barriers: infections of the lung and the gut. *Mucosal Immunol* 2009, 2, 100–102 <https://doi.org/10.1038/mi.2008.79>
31. Mönkemüller, K.; Fry, L.; Rickes, S. COVID-19, coronavirus, SARS-CoV-2 and the small bowel. *Rev Esp Enferm Dig.* 2020, 112, 383-388. doi: 10.17235/reed.2020.7137/2020.
32. Pan, Lei; Mu, Mi; Yang, Pengcheng; Sun, Yu; Wang, Runsheng; Yan, Junhong; Li, Pibao. Clinical characteristics of COVID-19 patients with digestive symptoms in Hubei, China. *Am. J. Gastroenterol.* 2020, doi: 10.14309/ajg.0000000000000620.
33. Wu, Yongjian.; Guo, Cheng; Tang, Lantian; Hong, Zhongsi; Zhou, Jianhui; Dong, Xin; Yin, Huan. Prolonged presence of SARS-CoV-2 viral RNA in Faecal samples. *The Lancet. Gastroenterology & Hepatology.* 2020, 5, 434–435.
34. Xiao, Fei.; Tang, Meiwen; Zheng, Xiaobin.; Liu, Ye; Li, Xiaofeng; Shan, Hong. Evidence for gastrointestinal infection of SARS-CoV-2. *Gastroenterology.* 2020, doi: 10.1053/j.gastro.2020.02.055. March.
35. Mesoraca, A.; Margiotti, K.; Viola, A. *et al.* Evaluation of SARS-CoV-2 viral RNA in fecal samples. *Virol J* 2020, 17, 86 <https://doi.org/10.1186/s12985-020-01359-1>
36. Jones, D.L., Baluja, M.Q., Graham, D.W., Corbishley, A.; McDonald, J.E.; Malham, S.K., et al. Shedding of SARS-CoV-2 in feces and urine and its potential role in person-to-person transmission and the environment-based spread of COVID-19. *Sci Total Environ.* 2020, 749, 141364.
37. Paul, K.S. Chan; Ka-Fai, To; Anthony, W.I. Lo; Jo, L.K. Cheung; Ida, Chu; Florence, W.L. Au; Joanna, H.M. Tong; John, S. Tam; Joseph, J.Y. Sung; Ho-Keung, Ng Persistent infection of SARS coronavirus in colonic cells in vitro *J Med Virol.* 2004, 74(1), 1–7. Published online 2004 Jul 13. doi: 10.1002/jmv.20138
38. Zuercher, A. W.; Coffin, S.E.; Thurnheer, M. C.; Fundova, P.; Cebra, J.J.; Nasal-Associated Lymphoid Tissue Is a Mucosal Inductive Site for Virus-Specific Humoral and Cellular Immune Responses. *The Journal of Immunology* 2002, vol. 168 , no. 4, 1796-1803; DOI: 10.4049/jimmunol.168.4.1796
39. Chua, R.L.; Lukassen, S.; Trump, S. et al. COVID-19 severity correlates with airway epithelium–immune cell interactions identified by single-cell analysis. *Nat Biotechnol.* 2020, 38, 970–979 . <https://doi.org/10.1038/s41587-020-0602-4>
40. Mironova, T.E.; Afonyushkin, V.N.; Kozlova, Yu.N.; Bobikova, A.S.; Koptev, V.Yu.; Cherepushkina, V.S.; Sigareva, N.A.; Kolpakov, F.A. Study of the protective effects of virucidal drugs on the model of coronavirus pneumonia. *Veterinary medicine and feeding.* 2020, 7, 35-38. DOI: 10.30917/ATT-VK-1814-9588-2020-7-10
41. Nefedova, E.; Koptev, V.; Bobikova, A.S.; Cherepushkina, V.; Mironova, T.; Afonyushkin, V.; Shkil, N.; Donchenko, N.; Kozlova, Y.; Sigareva, N.; Davidova, N.; Bogdanchikova, N.; Pestryakov, A.; Toledano-Magaña, Y. The Infectious Bronchitis Coronavirus Pneumonia Model Presenting a Novel Insight for the SARS-CoV-2 Dissemination Route. *Vet. Sci.* 2021, 8, 239. <https://doi.org/10.3390/vetsci8100239>
42. Afonyushkin, V.N.; Cherepushkina, V.S.; Tatarchuk, O.P.; Frolova, O.A. Study of anti-phage activity of disinfectants as a factor of suppressing horizontal gene transfer. *Bull. KSAU* 2020, 4, 88–96.

43. Afonyushkin, V.N.; Shirshova, A.N.; Shamovskaya, D.V.; Plomodyalov, D.N. A study of the antiviral effect of drug triviron on IBV. *Veterinary* 2018, 24–28. Available online: <https://agris.fao.org/agris-search/search.do?recordID=RU2019000107> (accessed on 11 October 2021).

44. Romo-Quíñonez, C.R.; Álvarez-Sánchez, A.R.; Álvarez-Ruiz, P.; Chávez-Sánchez, M.C.; Bogdanchikova, N.; Pestryakov, A.; Mejia-Ruiz, C.H. Evaluation of a new Argovit as an antiviral agent included in feed to protect the shrimp *Litopenaeus vannamei* against White Spot Syndrome Virus infection. *PeerJ* 2020, 8, e8446

Authors

Afonyushkin, V.N., Candidate of Biological Sciences, Head. Department of Molecular Biology, Siberian Federal Scientific Center of Agrobiotechnology RAS, Krasnoobsk, Russia. E-mail: lisocim@mail.ru; ORCID 0000-0001-5177-4733

Akberdin I.R., PhD in mathematical biology, Research Fellow, LTD “Biosoft.RU”, Novosibirsk Russia; Senior Research Fellow, Sirius University, Sochi, Russia; Senior Lecturer, Information Biology Section, Department of Natural Sciences, Novosibirsk National Research State University, Novosibirsk, Russia. E-mail: akberdinir@biosoft.ru; ORCID 0000-0003-0010-8620

Shchukin I.A. student Faculty of Mechanics and Mathematics, Novosibirsk National Research State University, Novosibirsk, Russia. E-mail: vashukin@bk.ru; ORCID

Mironova T.E. Junior Researcher, Sector of Molecular Biology, Siberian Federal Scientific Center of Agrobiotechnology RAS, Krasnoobsk, Russia. E-mail: mironova.tanya1994@mail.ru; ORCID 0000-0003-0860-1778

Kozlova Yu.N., Ph.D. Junior Researcher, Federal State Budgetary Institution of Science Institute of Chemical Biology and Fundamental Medicine SB RAS. E-mail: ulona79@mail.ru; ORCID 0000-0003-0811-8110

Bobikova A.S., junior researcher, Siberian Federal Scientific Center of Agrobiotechnology RAS, Krasnoobsk, Russia. E-mail: bobikova.anna97@gmail.com; ORCID 0000-0003-3198-3196

Kolpakov F.A., Candidate of Biological Sciences, Head of the Laboratory of Bioinformatics, Federal Research Center for Information and Computing Technologies, Novosibirsk, Russia. E-mail: fkolpakov@gmail.com; ORCID 0000-0002-0396-0256

Donchenko N.A. member corr. RAS Head of the Institute of Experimental Veterinary Medicine of Siberia and the Far East, Siberian Federal Scientific Center of Agrobiotechnology RAS, Krasnoobsk, Russia. E-mail: tbc2009@yandex.ru; ORCID 0000-0002-0885-0515

Cherepushkina V.S., Junior Researcher, Federal State Budgetary Institution of Science Siberian Federal Center for Agrobiotechnology RAS. E-mail: vicky88@bk.ru; ORCID 0000-0002-3378-7335

Poletaeva Yu. E. Ph.D. Junior Researcher, Federal State Budgetary Institution of Science Institute of Chemical Biology and Fundamental Medicine SB RAS. E-mail: ORCID 0000-0003-4211-0892

Corresponding author: Afonyushkin Vasily Nikolaevich, Cand. biol. Head of Science Sector of Molecular Biology, SFSCA RAS

Siberian Federal Scientific Centre of Agro-BioTechnologies of the Russian Academy of Sciences

Address: ICBFM SB RAS, 8 Lavrentiev Avenue, Novosibirsk, 630090, Russia.

+79231176461, e-mail: lisocim@mail.ru